Science Advances
AAAS

advances.sciencemag.org/cgi/content/full/5/5/eaaw0536/DC1

Supplementary Materials for

Wearable thermoelectrics for personalized thermoregulation

Sahngki Hong, Yue Gu, Joon Kyo Seo, Joseph Wang, Ping Liu, Y. Shirley Meng, Sheng Xu*, Renkun Chen*

*Corresponding author. Email: shengxu@eng.ucsd.edu (S.X.); rkchen@ucsd.edu (R.C.)

Published 17 May 2019, *Sci. Adv.* **5**, eaaw0536 (2019)
DOI: 10.1126/sciadv.aaw0536

This PDF file includes:

Note S1. Theoretical analysis of thermal design parameters to achieve active cooling of TED on human skin

Our main strategy is to match the thermal impedance between the TED and the environment. This is illustrated by the thermal balance of the TED for active cooling, which requires $T_{bare} > T_c$, where T_{bare} is the bare skin temperature without a TED or garment and T_c is the skin (cold side) temperature with TED cooling (Fig. 1c in the main text).

On the bare skin without the TED or garment

$$Q_{skin} = h_{air}(T_{bare} - T_{air}) \tag{S1}$$

where Q_{skin} is the metabolic heat from the skin, h_{air} is the heat transfer coefficient to the, air and T_{air} is the temperature of the air.

On the cold (skin) and hot sides of the TED

$$Q_{skin} = Q_{P,c} - Q_{cond} - Q_J \tag{S2}$$

$$Q_{air} = Q_{P,h} - Q_{cond} + Q_J \tag{S3}$$

where $Q_{P,c}$ is the Peltier cooling effect ($Q_{P,c} = S \cdot I \cdot T_c$, where S is the Seebeck coefficient, I is the current, and T_c is the temperature of the cold side, i.e. the skin), Q_{cond} is the conductive heat from the hot to the cold sides of the TED ($Q_{cond} = G_{TED}(T_h - T_c)$, where G_{TED} is the thermal conductance of the TED and T_h is the temperature of the hot side), Q_J is the joule heating of the TED ($Q_J = 0.5I^2R$, where R is the resistance), Q_{air} is the heat dissipation to the air ($Q_{air} = h_{air}(T_h - T_{air})$), and $Q_{P,h}$ is the Peltier heating effect on the hot side ($Q_{P,h} = S \cdot I \cdot T_h$).

By combining Eqs. (S1) and (S2)

$$h_{air}(T_{bare} - T_{air}) = Q_{P,c} - G_{TED}(T_h - T_c) - Q_J \tag{S4}$$

We know $T_h > T_{air}$ since $Q_{air} > 0$, and $T_{bare} > T_c$ for the active cooling condition, which results in

$T_{bare} - T_{air} > T_c - T_h$. Then

$$G_{TED}(T_h - T_c) < h_{air}(T_h - T_c) + Q_{P,c} - Q_J \quad \text{(S5)}$$

Eq. (S5) can be summarized to

$$G_{TED} < h_{air} + \alpha \quad \text{(S6)}$$

where α is a function of $Q_{P,c}$, Q_J, T_h, and T_c. Eq. (S6) shows that a small G_{TED} is required relative to h_{air} for the active cooling. However, the thermal impedance mismatch between G_{TED} and h_{air} of commercial TEDs is large: commercial TEDs has G_{TED} greater than 1000 W m^{-2} K^{-1}, and h_{air} on the TED without heat sink under a typical indoor condition is 10 – 20 W m^{-2} K^{-1}. Therefore, these devices only work when there is an efficient heat sink (e.g., fin or fan), but the bulky heat sinks render the TEDs non-wearable.

Note S2. Theoretical verification of the hot side temperature and heat flux during TED cooling on human skin

Based on the IR image on the hot side of the TED ($T_h = 42$ ℃, Fig. 5c) and the measured air temperature ($T_{air} = 24$ ℃), the heat flux from the hot side of the TED to the ambient (Q_{air}) is

$$Q_{air} = h_{air}(T_h - T_{air}) \quad \text{(S7)}$$

For $h_{air} = 11\ W\ m^{-2}\ K^{-1}$, Q_{air} is estimated to be 198 W m^{-2}. The heat flux dissipated to the hot side of the TED (Q_{TED}) has three components: metabolic heat from the skin (Q_{skin}), Peltier effect, and Joule heating of the TED

$$Q_{TED} = Q_{skin} + (N \cdot S \cdot I(T_h - T_{skin}) + I^2R)/A \quad (S8)$$

where $Q_{skin} = 87\ W\ m^{-2}$, N is the number of TE pillars ($N = 142$), S is the average Seebeck coefficient to the n and p type TE pillars, R is the total resistance of a TE device, I is the applied current (0.16 A during the experiment shown in Fig. 5c), T_{skin} is the measured skin temperature (30℃), and A is the area of the TED (5×5 cm^2). According to the characterization results of the TED shown in Fig. 2 in the main manuscript, $S = 196\ \mu V\ K^{-1}$, $R = 7.9\ \Omega$. Therefore, Q_{TED} is calculated to be $200\ W\ m^{-2}$. This heat flux is very close to the one estimated based on the heat dissipation from the hot side of the TED to the air (Q_{air} in Eq. S7). Therefore, we can conclude that our modeling and experiments are reliable.

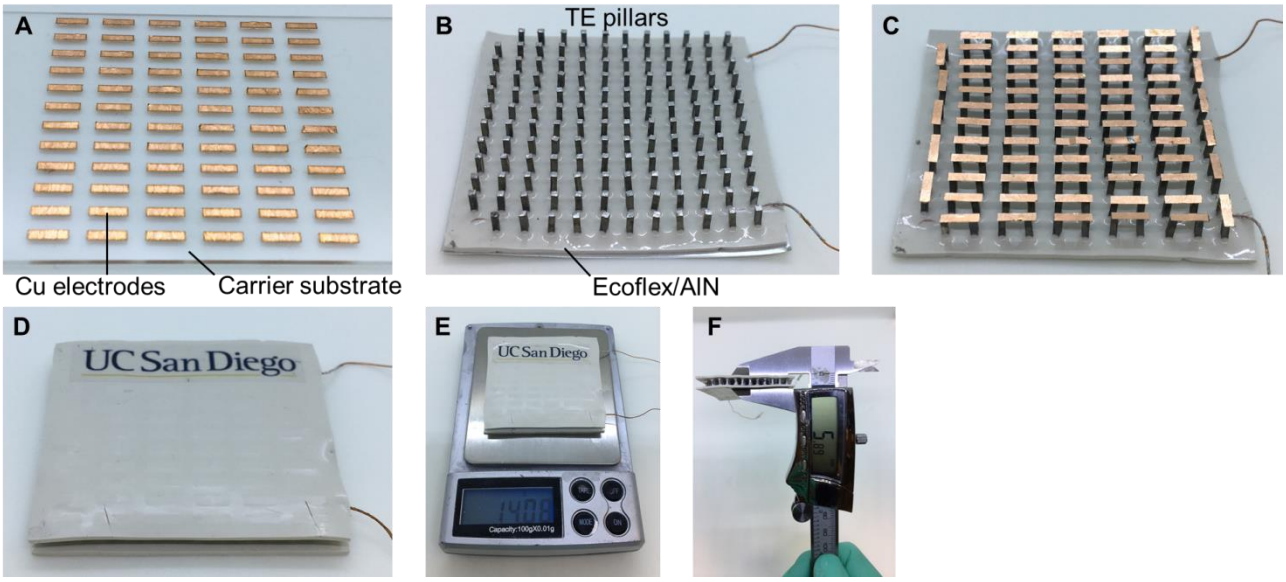

Fig. S1. Fabrication and characterization of the TED. (**A**) A carrier substrate with an array of copper electrodes. (**B**) An array of 142 TE pillars with the fabricated bottom layer including copper electrodes and AlN particles embedded in an Ecoflex stretchable sheet. (**C**) Soldered copper electrodes on the TE pillars. (**D**) Fabricated flexible TED by curing and cutting the Ecoflex/AlN mixture sheet. (**E**) Weight of the TED (14.1 g per device). (**F**) Thickness of the TED (~6 mm). Photo Credit: Sahngki Hong, UC San Diego.

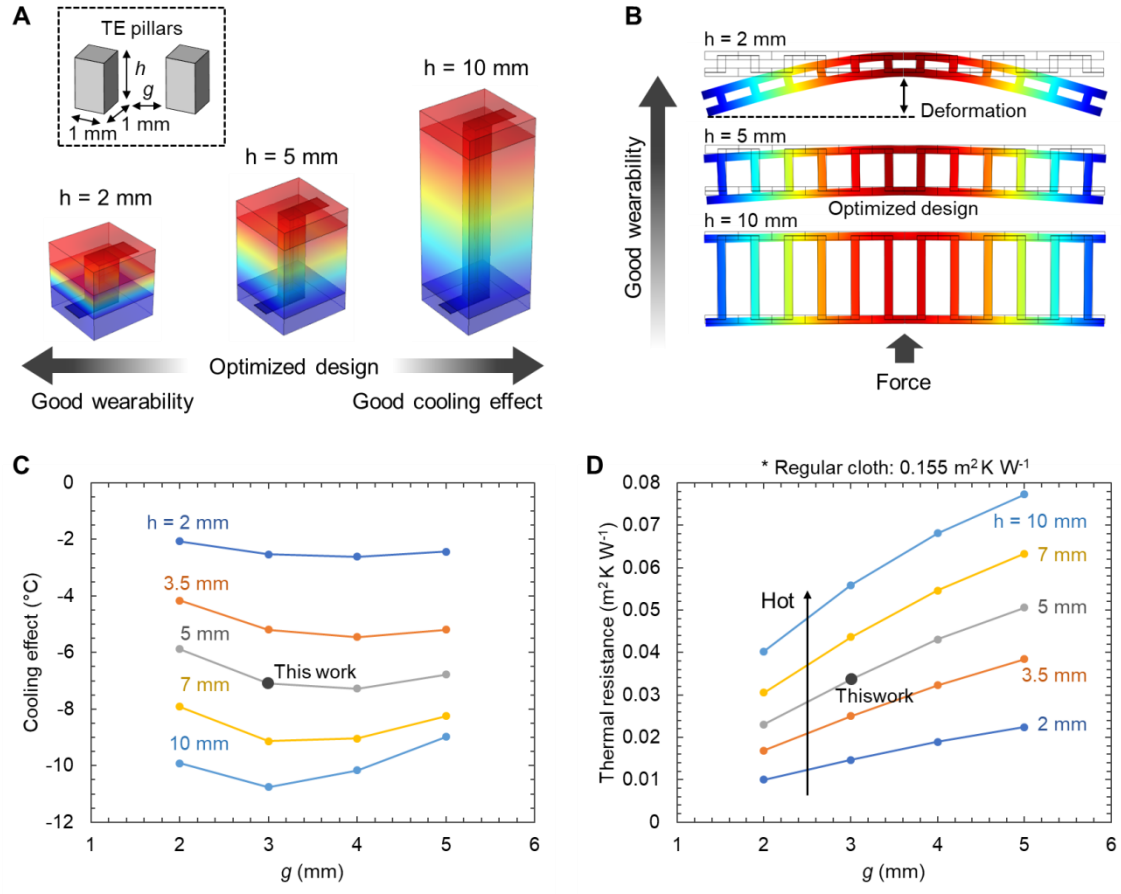

Fig. S2. Optimization of the TED. (**A**) Heat transfer model in COMSOL to optimize the TED design. The model used various geometric parameters for the optimization including the height of TE pillars (h = 2, 3.5, 5, 7, and 10 mm) and the gap between TE pillars (g = 2, 3, 4, and 5 mm). (**B**) Mechanical model in COMSOL used in Fig. 1E. Bending stiffness was simulated by applying a force and monitoring the corresponding deformation. (**C**) Maximum cooling effects with various TE pillar height and TE gap (g) values. The cooling effect was enhanced with increasing h up to 10 mm while there was an optimum g to maximize the cooling effect. However, the h also has to be optimized since a large h resulted in poor wearability as shown in (B) and Fig. 1E. (**D**) The thermal resistance of TED with various h and g values. Larger h and g values led to higher thermal resistance of the TED impeding heat dissipation and skin thermal comfort at hot environment when the TED is not operating. Our TED design with h = 5 mm and g = 3 mm showed a thermal resistance of 0.035 m^2 K W^{-1}, which is only ~20% of the resistance of regular clothes (0.155 m^2 K W^{-1}).

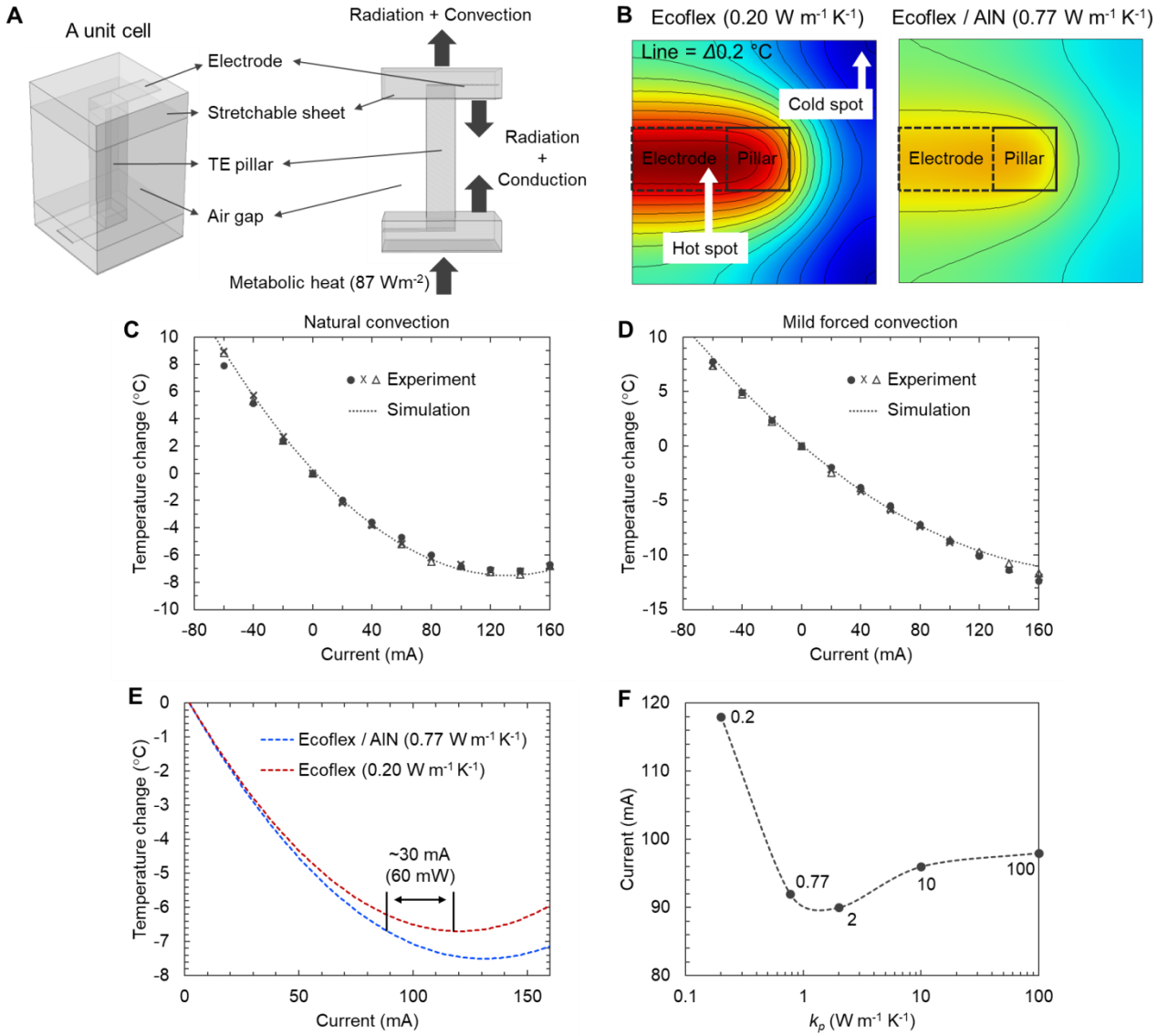

Fig. S3. COMSOL modeling of the TED cooling effect. (**A**) A unit cell of the TED with 1-mm thick top and bottom stretchable sheets, a TE pillar (1×1×5 mm), Cu electrodes (35 μm in thickness), and a 4-mm thick air gap. An empirical equation ($h_{conv} = 1.32(\Delta T/L)^{0.25}$) was applied to model the natural convection heat transfer to the air, where $\Delta T = T_h - T_{air}$, T_{air} is the ambient temperature, and L is the characteristic length. A heat flux of 87 W m^{-2} from the bottom of TED was used as the metabolic heat from a human body. Radiation between the cold and hot sides was also considered in addition to the conduction through the air gap since the radiation accounts for ~40% of the total heat transfer in the air gap. (**B**) Simulation results of temperature distribution in the heat spreading layers, made of either pristine Ecoflex (left) or an Ecoflex/AlN mixture (right). The pristine Ecoflex showed up to 2.7 °C temperature variations within the sheet, whereas the Ecoflex/AlN mixture had ~0.7 °C maximum temperature difference. (**C**) Comparison of experimental results and the simulation result under a natural convection condition. (**D**) Comparison of experimental results and the simulation result under a mild forced convection condition with ~5 km h^{-1} wind. Three

experimental data points at each applied electric current were plot together in (C) and (D) and showed excellent match with the simulation result. The root mean square error of the experimental data points was less than 0.3 °C. (**E**) Simulation results of cooling effect with Ecoflex and Ecoflex/AlN mixture heat spreading layers. The high thermal conductivity of Ecoflex/AlN mixture layer reduces the power consumption of the TED by up to 40% (from 140 mW to 80 mW) at 6.6 °C of TED cooling effect. (**F**) Simulation results of power consumption at 6.6 °C of TED cooling effect with various thermal conductivity of the stretchable sheet (k_p). The results indicate that the power consumption of the TED with Ecoflex/AlN mixture layer (k_p = 0.77 W m^{-1} K^{-1}) almost reaches the minimum value. It is worth noting that the power consumption increase with the k_p higher than ~1.5 W m^{-1} K^{-1}, which is similar to the thermal conductivity of TE pillars, is because the heat flow through TE pillars easily dissipates at the interface of TE pillars and the stretchable sheets, and 0.5-mm-long segment of TE pillars embedded in the stretchable sheets cannot contribute the thermal insulation between cold and hot sides anymore.

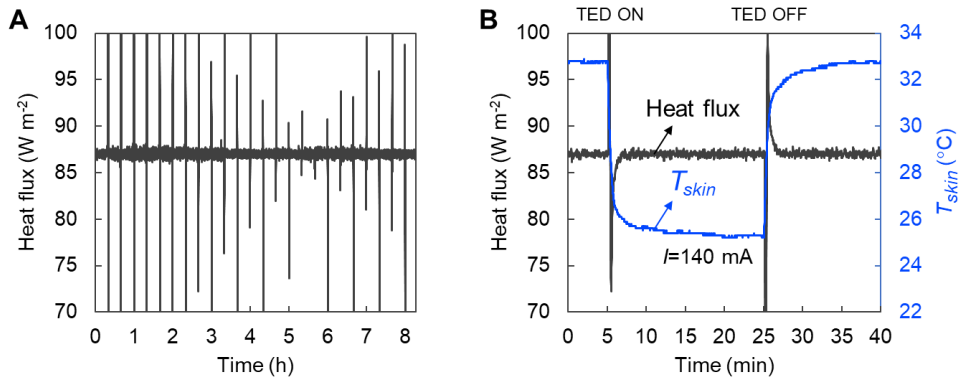

Fig. S4. PID control of the heat flux from the heater. (**A**) Measured heat flux applied to the heater during cooling/heating measurement. The heating power was maintained at a constant 87 W m^{-2} value using a PID controller, with the feedback from the heat flux sensor. (**B**) An example of heat flux recovery graph with the PID controller after switching on/off the TED. When the TED was switched on at the electrical current of 140 mA, the cooling of the T_{skin} increased the heat flux from the insulation layer to the TED bottom. On the contrary, switching off the TED decreased the heat flux. The PID controller recovered the heat flux within two minutes.

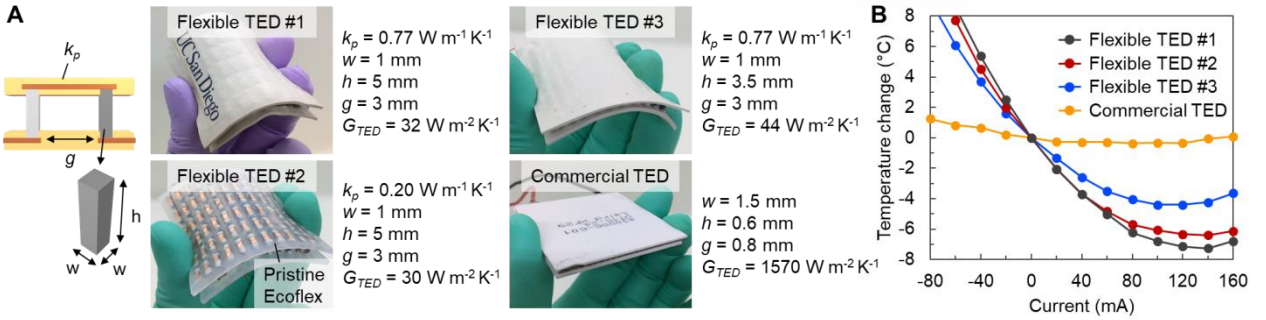

Fig. S5. Comparison of TEDs. (**A**) Four TEDs with various TE pillar designs and thermal conductivity values of the stretchable polymer sheets (k_p). The four devices included three flexible TEDs and a commercial TED made of the same TE materials. The geometric and thermal parameters of the TEDs are summarized in the schematics. (**B**) Summary of cooling/heating effects. The flexible TEDs showed the maximum cooling of 4.6 °C (blue), 6.3 °C (red), and 7.3 °C (black) while the commercial TED (yellow) did not show any cooling effect. The significantly improved cooling in the flexible TEDs is attributed to our optimal thermal design featured with low G_{TED}. Photo Credit: Sahngki Hong, UC San Diego.

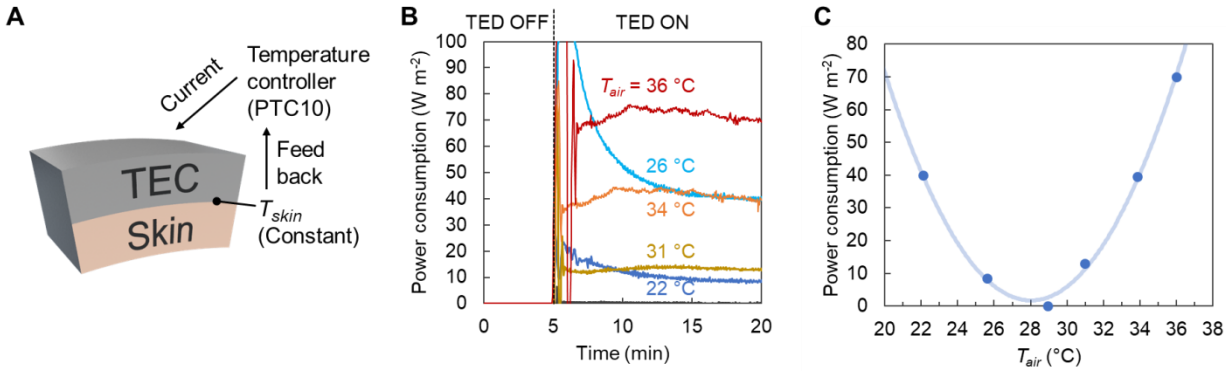

Fig. S6. Measurement system and power consumption of the thermoregulation on human skin. (**A**) Schematic of measurement system for thermoregulation by the TED on human skin. (**B**) Power consumption of the TED during thermoregulation at various air temperatures T_{air}. (**C**) Summary of the power consumption as a function of T_{air}.

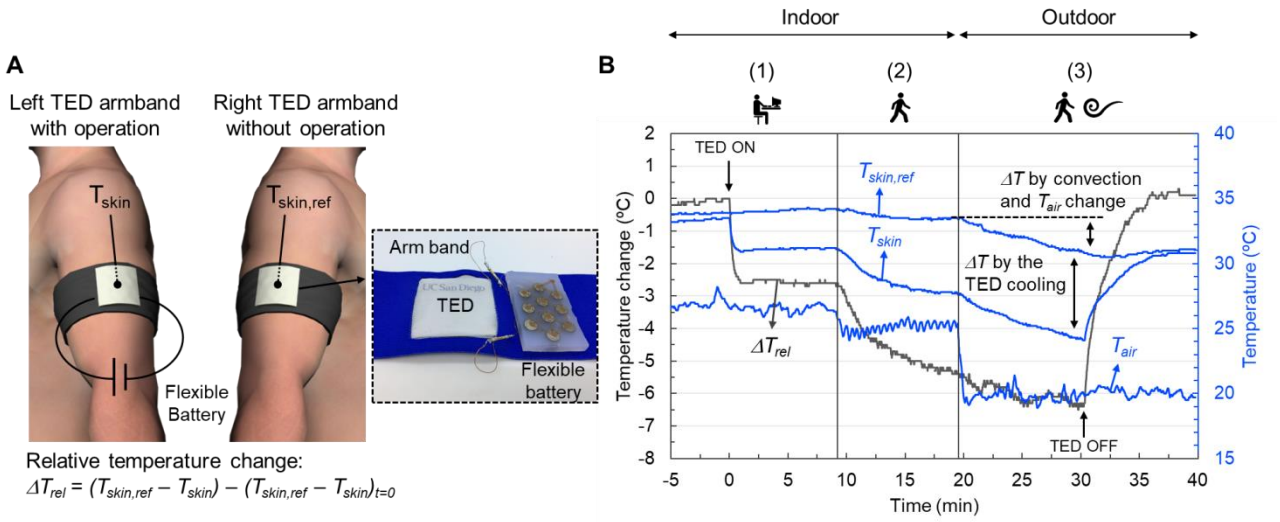

Fig. S7. Temperature change during the mobile thermoregulation demonstration. (**A**) Schematics of the demonstration setup with two identical TED armband worn on both arms, but the TED on the left armband was operating (i.e., applied with current from the flexible battery) and the other TED on the right armband was not operationg and used as a reference. The relative temperature change was determined by subtracting T_{skin} from $T_{skin,ref}$ to exclude possible skin temperature changes caused by changes in air temperature, convection heat transfer coefficients, and metablic rates. The inset shows the integrated TED arm band with the flexible battery pack shown in Fig. 5f in the main text. (**B**) Measured temperature during the demonstration. T_{skin} and $T_{skin,ref}$ were almost the same before and after demonstration because the TED armbands and heat generation from both arms are identical. $T_{skin,ref}$ drifted as changing thermal conditions, and compensate the change to extract the active cooling effect from the TED. Photo Credit: Sahngki Hong, UC San Diego.